DOI: 10.1002/ejic.200600423

Hydroxyapatite Nanocrystals Modified with Acidic Amino Acids

Elisa Boanini,[a] Milena Fini,[b] Massimo Gazzano,[c] and Adriana Bigi*[a]

Keywords: Hydroxyapatite / Amino acids / Nanocrystals

HA-aspartic acid (HA-ASP) and HA-glutamic acid (HA-GLU) composite nanocrystals were synthesized in aqueous medium. The relative amino acid content, determined through HPLC analysis, increases with the amino acid concentration in solution up to a maximum of about 7.8 wt.-% for HA-ASP and 4.3 wt.-% for HA-GLU composites. The dimensions of the composite nanocrystals decrease on increasing the amino acid content. The line profile analysis of the X-ray diffraction reflections was performed using: (i) the Scherrer method, (ii) the Warren–Averbach approach, and (iii) the Rietveld refinement. The results indicate that the broadening of the diffraction peaks is partly due to the decrease of crystallite size on increasing amino acid content, and even more to the simultaneous increase of microstrain. The different extent of structural disorder induced by the two amino acids, in agreement with their different incorporation, suggests a greater affinity of aspartic acid for hydroxyapatite structure.

Introduction

The idea of mimicking designs from nature and adopting the same strategies as those utilized by living organisms to produce functional structures has entered into many areas of applied science, most notably the synthesis of new materials.[1] The biomimetic strategy is based on the principle that nucleation and growth of inorganic crystals in biological environments occurs in the presence of biological macromolecules, which may be linked to structural organic matrices or secreted as soluble polyelectrolytes in the mineralization environment.[2,3] Control occurs through specific or nonspecific interactions of biological macromolecules with the charged surfaces of the growing inorganic crystals.[3–5] This has prompted a number of studies on the preparation of hydroxyapatite nanocrystals in the presence of biomolecules.[6–8] Proteins and macromolecules, which are most active in the mediation of biologically directed mineral growth, contain amino acid residues, specifically regions rich in carboxylates, that interact with mineral surfaces.[9–11] In bone, nucleation and growth of apatite crystals involve proteins containing high amounts of aspartic and glutamic acid residues.[12] Both glutamic and aspartic acids have been reported to induce osteoblast differentiation and to increase extracellular mineralization.[13–15]

[a] Department of Chemistry "G. Ciamician", University of Bologna,
Via Selmi 2, 40126 Bologna, Italy
Fax: +39-51-2099456
E-mail adriana.bigi@unibo.it
[b] Experimental Surgery Department, Research Institute Codivilla Putti, Rizzoli Orthopaedic Institute,
Bologna, Italy
[c] ISOF-CNR, c/o Department of Chemistry "G. Ciamician", Bologna, Italy

We have recently demonstrated the possibility of synthesizing hydroxyapatite, $Ca_{10}(PO_4)_6(OH)_2$ (HA), containing aspartic acid (HA-ASP) and HA containing glutamic acid (HA-GLU), and we have verified that the presence of the acidic amino acids in the composite nanocrystals favours osteoblast proliferation and promotes their metabolism and differentiation.[16] Understanding how these amino acids interact with HA structure, and clarifying their role in the control of the properties of the HA crystals is of interest both for the development of biomaterials suitable to repair the skeletal system, as well as for a better understanding of the natural processes. To this aim, we have carried out a structural, morphological and chemical investigation of hydroxyapatite nanocrystals synthesized in the presence of increasing amounts of aspartic acid and of glutamic acid.

Results and Discussion

Sample Characterization

The powder X-ray diffraction patterns of the products synthesized in the presence of L-aspartic acid or L-glutamic acid indicate that they are constituted of hydroxyapatite as a unique crystalline phase. However, glutamic acid, and even more so aspartic acid, provokes a broadening of the diffraction peaks, which increases on increasing the amino acid concentration in solution, as is appreciable in the patterns shown in Figure 1. The reduction of the degree of crystallinity is confirmed by the results of the FT-IR absorption analysis. In fact, the FT-IR spectra of the products obtained in the presence of increasing concentration of amino acid show a decrease of the relative intensity of the absorption bands at 3572 and 630 cm^{-1}, caused by OH^-

stretching and libration mode, respectively (Figure 2). Moreover, the spectra of HA samples prepared in the presence of an amino acid display, other than the bands characteristic of the hydroxide and phosphate groups, several absorption bands in the range 1700–1400 cm^{-1}, which are indicative of the presence of the amino acids, as can be observed for sample HA-GLU 0.20 in part b of Figure 2. This region of the spectra is quite different from that present in the previously reported spectra of mechanical mixtures containing HA and ASP or GLU, which display a number of bands due to the two discrete components of the mixture.[16] In particular, the broad absorption band centred at 1568 cm^{-1} (1591 cm^{-1} in the HA-ASP spectra) can be attributed to glutamic acid (aspartic acid). The small shift with respect to the position characteristic of the carboxylic stretching band in the free amino acids is in agreement with an increase of the C–O bond length due to interaction with the apatitic phase.[17] Table 1 reports the relative amount of amino acid determined through HPLC and expressed as wt.-% of the solid product. The relative quantity of amino acid in the crystals increases with the amino acid concentration in solution up to a maximum of about 7.8 wt.-% for HA-ASP and 4.3 wt.-% for HA-GLU composites. Aspartic acid incorporation into HA nanocrystals is always greater than that of glutamic acid, suggesting a greater affinity of aspartic acid for hydroxyapatite structure. Amino acid incorporation does not significantly affect the stoichiometry of hydroxyapatite as it can be deduced also from the Ca/P molar ratio of the composites which assumes a mean value of 1.68 ± 0.03, very close to the stoichiometric value of 1.67, independently from the amino acid content. On the contrary, the dimensions of the crystals are strongly affected by the presence of both aspartic and glutamic acid. In Figure 3, a TEM micrograph of HA crystals is compared with that of HA-amino acid composite crystals. Hydroxyapatite is constituted of platelet-shaped crystals with mean dimensions up to about 200 × 40 nm, elongated along a direction parallel to the crystallographic *c*-axis (Figure 3, a), whereas composite nanocrystals display definitely smaller dimensions (Figure 3, b–d). The dimensions decrease on increasing the amino acid content, in agreement with the reduction of the degree of crystallinity. Furthermore, the crystals with higher amino acid content, which display mean dimensions of about 50 × 10 nm, should be also extremely thin as they appear very transparent to the electron beam. In a previous study on the interaction of poly-L-aspartate with HA, we verified a remarkable increase of the length/width ratio of the composite crystallites, in agreement with a preferential adsorption of the polyamino acid on the crystal faces parallel to the *c*-axis.[18] At variance, the significant reduction of the dimensions along all the three directions induced by ASP and GLU suggests a nonspecific interaction with the HA crystal faces, and it might be interpreted as indicating

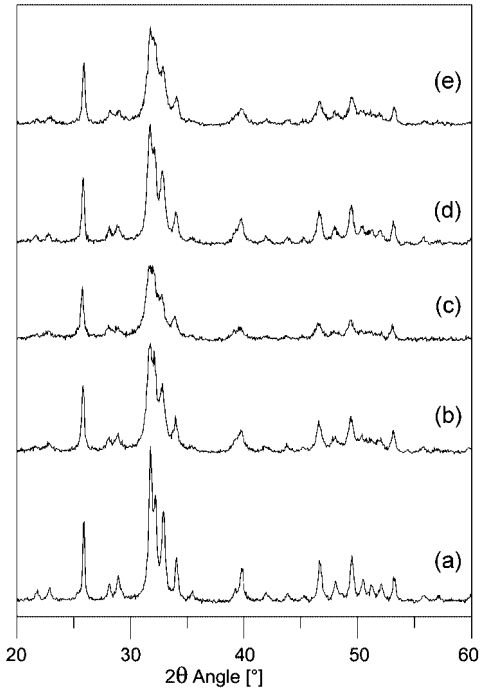

Figure 1. Powder X-ray diffraction patterns of hydroxyapatite synthesized in the absence of amino acid (a); in the presence of aspartic acid 0.10 M (b) and 0.20 M (c) and in the presence of glutamic acid 0.10 M (d) and 0.20 M (e).

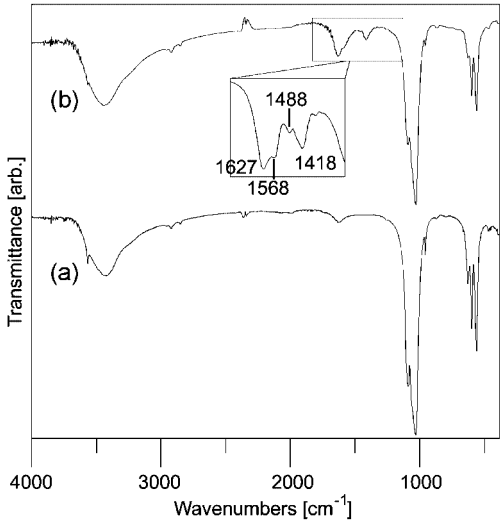

Figure 2. FT-IR adsorption spectra of the HA samples prepared in the absence of amino acid (a) and in the presence of glutamic acid 0.20 M (b). The absorption bands in the zoomed range 1700–1400 cm^{-1} can be attributed to glutamic acid.

Table 1. Amount of amino acid associated to the inorganic phase evaluated through HPLC and expressed as wt.-% of the solid product.

Amino acid concentration in solution [M]	Aspartic acid content [wt.-%]	Glutamic acid content [wt.-%]
0	–	–
0.05	3.14	1.17
0.10	4.28	2.50
0.15	5.35	3.30
0.20	7.80	4.30

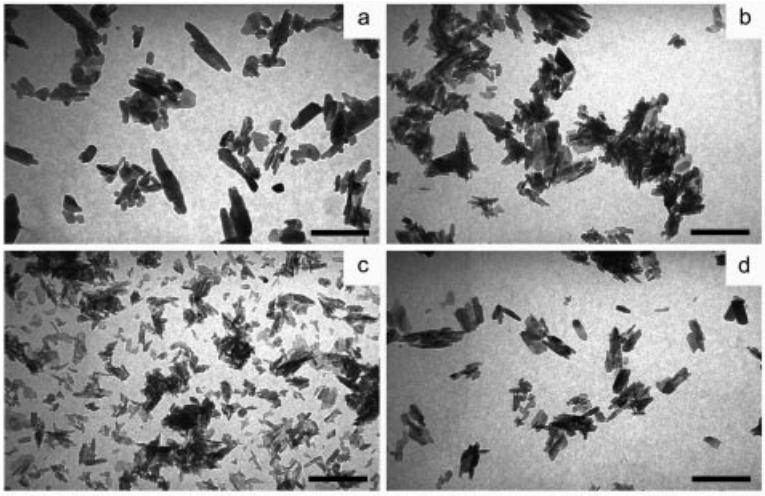

Figure 3. TEM micrographs of HA crystals synthesized in the absence of amino acid (a); in the presence of aspartic acid 0.10 M (b) and 0.20 M (c) and in the presence of glutamic acid 0.20 M (d). Scale-bar = 200 nm.

that the presence of the amino acids provokes an increase of the nucleation rate that, as a consequence, leads to a growth reduction.[15] Aspartic and glutamic acid seem to exert a similar control on crystal dimensions, as can be deduced from the comparison of Figure 3 (parts b and d).

In agreement with the crystal dimensions, the values of the specific surface area, determined applying the Brunauer–Emmett–Teller (BET) theory and reported in Table 2 increases as a function of amino acid content, up to 114 $m^2 g^{-1}$, which represents a very high value for synthetic platelet-like hydroxyapatite crystals.

Table 2. Surface areas of hydroxyapatite samples synthesized in the presence of different amino acid concentrations in solution.

Sample	Surface area [$m^2 g^{-1}$]
HA	60
HA-ASP 0.10	84
HA-ASP 0.20	114
HA-GLU 0.10	78
HA-GLU 0.20	86

Crystallographic Investigation

Line profile analysis has been applied in order to investigate the line broadening increase observed in the XRD patterns of the samples synthesized in the presence of increasing amounts of amino acid (Figure 1).

A qualitative estimation of the size of coherently scattering domains (i.e., the crystallite size) as derived from the Scherrer equation, on the hypothesis of negligible microstrain, is reported in Table 3. τ_{002} is related to the mean crystallite size along the *c*-axis whereas τ_{310} refers to the mean crystal size along a direction perpendicular to it.

Table 3. Coherent lengths (τ_{hkl}) of the perfect crystalline domains in the direction normal to 002 and to 310 planes calculated using the Scherrer method.

Sample	τ_{002} [nm]	τ_{310} [nm]
HA	44.3(9)	22.4(6)
HA-ASP 0.05	38.9(7)	17.0(3)
HA-ASP 0.10	35.8(3)	15.5(2)
HA-ASP 0.15	35.2(3)	14.8(3)
HA-ASP 0.20	29.8(4)	11.3(3)
HA-GLU 0.05	43.8(9)	19.9(3)
HA-GLU 0.10	35.8(6)	15.2(2)
HA-GLU 0.15	34.6(3)	14.7(3)
HA-GLU 0.20	33.7(3)	12.0(3)

The crystal sizes decrease as the aspartic or glutamic acid content increases. The contraction appears to be greater along the direction orthogonal to the *c*-axis, similarly to what was previously found for poly-L-aspartate.[18] The comparison with the data reported in Table 1 indicates that GLU incorporation provokes a greater contraction of crystal size.

In general, the nature of imperfections responsible for the broadening of the diffraction peaks could be due to (i) a reduction of the crystallite domains, (ii) the occurrence of still large domains but with lattice spacings that differ one from another, and (iii) the presence of elastic deformations and stacking faults inside the domains. In order to evaluate the relative contribution of crystallite size and microstrain to the diffraction peak broadening, some selected samples were submitted to the Warren–Averbach analysis. The analysis was performed on two pairs of reflections (002/004 and 111/222). The results are reported in Table 4. Since only two pairs of peaks were analysed, the results are rather semi-quantitative. However, the data clearly show that both amino acids provoke a reduction of the mean crystallite size, without significant differences along the two investigated directions.

Table 4. Microstructural parameters calculated using Warren–Averbach analysis.

Sample	002/004				111/222			
	$\langle D \rangle_s$ (nm)	$\langle D \rangle_v$ (nm)	$\langle \varepsilon_L^2 \rangle^{\frac{1}{2}}$ ($\times 10^3$)	$\left\langle \varepsilon^2_{\frac{\langle D \rangle_V}{2}} \right\rangle^{\frac{1}{2}}$ ($\times 10^3$)	$\langle D \rangle_s$ (nm)	$\langle D \rangle_v$ (nm)	$\langle \varepsilon_L^2 \rangle^{\frac{1}{2}}$ ($\times 10^3$)	$\left\langle \varepsilon^2_{\frac{\langle D \rangle_V}{2}} \right\rangle^{\frac{1}{2}}$ ($\times 10^3$)
HA	38.7	28.6	1.34	1.57	27.7	26.4	0.97	0.93
HA-ASP 0.10	18.7	21.9	1.36	1.56	17.0	18.0	1.21	1.71
HA-ASP 0.20	11.3	11.6	1.33	2.55	9.8	10.4	1.43	2.81
HA-GLU 0.10	18.6	22.4	1.33	1.78	16.9	17.9	1.33	1.76
HA-GLU 0.20	14.7	18.7	1.59	2.73	9.7	12.1	1.53	2.82

$\langle D \rangle_s$, $\langle D \rangle_v$ are the mean sizes of crystallites weighed on the surface or volume

$\langle \varepsilon_L^2 \rangle^{\frac{1}{2}}$ is the root of mean-square lattice strain

Furthermore, all the composites show an increase of the microstrain parameters indicating that the incorporation of both amino acids provokes a significant decrease of crystal perfection, which is more evident for HA-GLU composites. The parameters obtained for the 111/222 planes are larger than those for the 002/004 planes suggesting a smaller amount of stacking faults along the *c*-axis. These data can be used to interpret the different results obtained with the Scherrer analysis. The Scherrer formula gives proper values of the mean crystallite size along the investigated direction only for strain-free samples. In spite of the different reflections analyzed by the Warren–Averbach method, the results clearly indicate that the microstrain contribution is smaller along the 00*l* direction than along the direction orthogonal to it. As a consequence, τ_{310} appeared more affected than τ_{002} simply because of the neglected microstrain contribution.

In order to verify the possible structural modifications, a full profile fitting was performed on XRD patterns of the two composites at the highest amino acid content (samples HA-ASP 0.20 and HA-GLU 0.20). The main steps of the procedure are reported in the experimental section and a comparison between the experimental and calculated pattern, as obtained at the end of the process, is reported in Figure 4 for the HA-aspartic acid sample. The final discrepancy factors *Rp* = 0.044, *Rwp* = 0.058 and *Rp* = 0.049, *Rwp* = 0.064 were achieved for HA-ASP 0.20 and HA-GLU 0.20, respectively. The results indicate that the cell parameters of the HA-amino acid composites are still the same as a stoichiometric HA [HA *a* = 0.9424(1) nm, *c* = 0.6880(1) nm; HA-ASP 0.20 *a* = 0.9427(7) nm, *c* = 0.6877(8) nm; HA-GLU 0.20 *a* = 0.9425(4) nm, *c* = 0.6884(4) nm]. The presence of an appreciable amorphous fraction in the samples has to be excluded, because leaving variable the integrated intensity of a bell-shaped curve superimposed on the background did not allow a better convergence. The Debvin program takes into account the anisotropy of the crystallite dimensions that can be used as variable parameters.[19] A good agreement index is reached when the mean value of the crystallite dimensions along the *c*-axis is almost double respect to the values along *a* and *b*, in agreement with the results of the Scherrer and Warren–Averbach analysis. No significant variation of the atomic positions and occupancy factors was detected, whereas an increase of about 20% in the thermal parameters seems to indicate an increased general disorder in the structure of the composites.

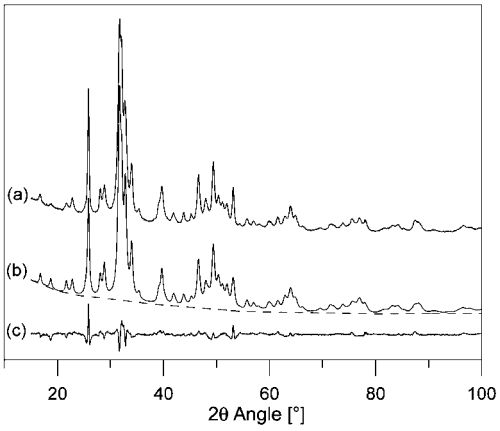

Figure 4. Comparison between the observed (a) and the calculated (b) powder diffraction patterns of HA-ASP 0.20. The dotted line is the background, while the line at the bottom (c) is the difference curve.

Conclusions

Composite HA-ASP and HA-GLU nanocrystals have been synthesized at different amino acid content. The presence of the amino acids in the reaction solution does not inhibit nucleation of HA, but reduces the growth of the composite nanocrystals in agreement with the increase of the surface area on increasing amino acid content. TEM images confirm the reduction of dimensions, which does not modify the morphology of the composite nanocrystals. Accordingly, the results of the structural analyses showed a major contribution from microstrain to the broadening of the diffraction peaks for both HA-ASP and HA-GLU. However, glutamic acid induces a greater disorder in the HA structure, most likely because of its bigger size, which

could justify the greater affinity of aspartic acid for HA suggested by its greater incorporation into the composite nanocrystals.

Experimental Section

The synthesis of hydroxyapatite was carried out under N_2 using a $Ca(NO_3)_2{\cdot}4H_2O$ (50 mL, 1.08 M) solution at pH adjusted to 10 with NH_4OH. The solution was heated at 90 °C and a $(NH_4)_2HPO_4$ solution (50 mL, 0.65 M), pH 10 adjusted with NH_4OH, was added dropwise whilst stirring. The precipitate was maintained in contact with the reaction solution for 5 h at 90 °C whilst stirring, then centrifuged at 10000 rpm for 10 min and repeatedly washed with CO_2-free distilled water. The product was dried at 37 °C overnight.

Hydroxyapatites at different amino acid contents were obtained by adding L-aspartic acid or L-glutamic acid (SIGMA) to the phosphate solution, before adjusting the pH to 10 with NH_4OH. The tested concentrations were 0.05, 0.10, 0.15 and 0.20 M.

X-ray diffraction analysis was carried out by means of a PANalytical X'Pert PRO powder diffractometer. Cu-K_α radiation was used (40 mA, 40 kV). The 2θ range was from 10 to 60° at a scanning speed of 0.75°min^{-1}. In order to evaluate the coherence lengths of the crystals and to perform the line profile analysis, further X-ray powder data were collected in step scanning mode with a fixed counting time of 10 s for each 0.030°/step.

For FT-IR adsorption analysis, the powdered samples (1 mg) were carefully mixed with KBr (250 mg, infrared grade) and pelletized under a pressure of 10 tons for 2 min. The pellets were analyzed with a Nicolet FT 205 IR spectrophotometer to collect 32 scans in the range 4000–400 cm^{-1} at a resolution of 4 cm^{-1}.

Amino acid contents were determined by means of HPLC, following a procedure reported elsewhere.[20] Briefly, to the starting solution containing the amino acid in HCl (10^{-2} M) was added an equal volume of borate buffer (0.2 M, pH 8) and then 9-fluorenylmethyl chloroformate (FMOC-Cl) solution (in CH_3CN). At the end of the time allowed for derivatization (typically 1 min), excess 1-aminoamantadine (ADAM) was added to prevent hydrolysis of excess FMOC-Cl to FMOC-OH. Before injection sample solutions were filtered through Teflon filters (0.2-μm porosity). Compounds were separated on a 250 × 4 mm i.d. 5-μm Purospher column from Merck. The HPLC pump was a Varian 9012 and the injection valve a Rheodyne 7525 equipped with a 13.2 μL calibrated loop. Compounds were detected with a Hewlett–Packard 1040 diode array detector. Data were acquired and processed with an HP 9000 Chemstation.

Calcium and phosphorus contents were determined by means of a Dionex DX100 chromatography system equipped with a Dionex CD20 conductivity detector. Powders were previously dissolved in HCl (0.1 M). The chromatographic data were collected and processed with the Dionex Peaknet 5.1 program.

For TEM investigations, a small amount of powder was dispersed in ethanol and submitted to ultrasonication. A drop of the calcium phosphate suspension was transferred onto holey carbon foils supported on conventional copper microgrids. A Philips CM 100 transmission electron microscope operating at 80 kV was used.

The surface area was measured using a Carlo Erba Sorpty 1750 BET analyser using constant volume N_2 absorption with desorption at 100 °C.

Line Profile Analysis

Scherrer Analysis: The line broadening of the 002 and 310 reflections was used to evaluate the length of the coherent domains (τ_{hkl}) along the *c*-axis and along a direction perpendicular to it. τ_{hkl} values were calculated from the widths at half maximum intensity ($\beta_{1/2}$) using the Scherrer equation (1)[21]

$$\tau_{hkl} = \frac{k\,\lambda}{\beta_{1/2}\cos\theta} \quad (1)$$

where λ is the wavelength, θ the diffraction angle and K a constant depending on crystal habit (chosen as 0.9). The silicon standard peak 111 was used to evaluate the instrumental broadening.

Warren–Averbach Analysis: The Warren–Averbach approach[21] was applied with the aim to separate the line broadening due to size effect from the strain contribution. The analysis was performed on two couples of reflections (002/004 and 111/222) by using the WinFit program.[22] A strain free LaB_6 NIST sample was used to take into account the instrumental broadening.

Rietveld Refinement Analysis: The DEBVIN program,[23] essentially implemented on the Rietveld routine,[24] was used to refine the structures of HA and HA-amino acid composites. The same space group ($P6_3$/m, *n*. 176), cell parameters, atomic positions and thermal parameters as those of the initial structural model of HA were introduced.[25] The background was treated as an empirical segmented line where the heights of the seven nodes are free variables. The peaks were fitted by using a Pearson VII function. Half width of the diffraction peaks as a function of 2θ was evaluated by the formulation of the Caglioti model.[26] Rietveld refinement was performed in several stages, the parameters obtained in each step being deferred in the following one. In the first cycles the scale factor and the background were refined. Refinement of the other parameters is in the following order: zero shift, profile parameters, asymmetry parameter and cell parameters. Refinements of the occupancy factors and of the coordinates were tested at the latest stages of the procedure, starting with those of the two metal sites. In the last refinement cycles the overall thermal parameter was released together with the other 14 variables.

Acknowledgments

This research was carried out with the financial support of MIUR (FIRB RBNE01458S_004), and the University of Bologna (Funds for Selected Research Topics).

[1] S. Mann, *Biomineralization. Principles and Concepts in Bioinorganic Materials Chemistry*, Oxford University Press, Oxford, **2001**.
[2] A. L. Boskey, *Calcif. Tissue Int.* **1998**, *63*, 179–182.
[3] L. Addadi, J. Moradian-Oldak, H. Furedi-Milhofer, S. Weiner, A. Veis, in *Chemistry and Biology of Mineralized Tissues* (Eds.: H. Slavkin, P. Price), Elsevier, The Netherlands, **1992**, pp. 153–162.
[4] A. Berman, L. Addadi, A. Kvick, L. Laiserovitz, M. Nelson, S. Weiner, *Science* **1990**, *250*, 664–667.
[5] S. Mann, B. R. Heywood, S. Rajam, J. D. Birchall, *Nature* **1988**, *394*, 692–695.
[6] R. Gonzalez-McQuire, J. Y. Chane-Ching, E. Vignaud, A. Lebugle, S. Mann, *J. Mater. Chem.* **2004**, *14*, 2277–2281.
[7] S. Tanaka, N. Shiba, M. Senna, *Sci. Technol. Adv. Mater.* **2006**, *7*, 226–228.
[8] S. Teng, J. Shi, B. Peng, L. Chen, *Compos. Sci. Technol.* **2006**, *66*, 1532–1538.

[9] C. S. Sikes, M. L. Yeung, A. P. Wheeler, in *Surface Reactive Peptides and Polymers: Discovery and Commercialization* (Eds.: C. S. Sikes, A. P. Wheeler), ACS Symposium Series XIII, ACS Books, Washington, DC, **1991**, p. 444.
[10] A. George, L. Bannon, B. Sabsay, J. W. Dillon, J. Malone, A. Veis, N. A. Jenkins, D. J. Gilbert, N. G. Copeland, *J. Biol. Chem.* **1996**, *271*, 32869–32873.
[11] S. R. Qiu, A. Wierzbicki, C. A. Orme, A. M. Cody, J. R. Hoyer, G. H. Nancollas, S. Zepeda, J. J. De Yoreo, *Proc. Natl. Acad. Sci. USA* **2004**, *101*, 1811–1815.
[12] G. K. Hunter, C. L. Kyle, H. A. Goldberg, *Biochem. J.* **1994**, *300*, 723–728.
[13] E. Hinoi, T. Takarada, Y. Yoneda, *J. Pharmacol. Sci.* **2004**, *94*, 215–220.
[14] D. J. Mason, *Eur. Cells Mater.* **2004**, *7*, 12–26.
[15] S. Sarig, *Bone* **2004**, *35*, 108–113.
[16] E. Boanini, P. Torricelli, M. Gazzano, R. Giardino, A. Bigi, *Biomaterials* **2006**, *27*, 4428–4433.
[17] A. Barth, *Prog. Biophys. Mol. Biol.* **2000**, *74*, 141–173.
[18] A. Bigi, E. Boanini, M. Gazzano, M. A. Kojdecki, K. Rubini, *J. Mater. Chem.* **2004**, *14*, 274–279.
[19] R. Millini, G. Perego, S. Brückner, *Mater. Sci. Forum* **1991**, *79–82*, 239–244.
[20] D. Melucci, M. Xie, P. Reschiglian, G. Torsi, *Chromatographia* **1999**, *49*, 317–320.
[21] H. P. Klug, L. E. Alexander, *X-ray Diffraction Procedures for Polycrystalline and Amorphous Materials*, Wiley Interscience, New York, **1974**.
[22] S. Krumm, Proceedings of the XIIIth Conference on Clay Mineralogy and Petrology, Praha, in *Acta Universitatis Carolinae Geologica*, **1994**, *38*, 253–261.
[23] A. Immirzi, *Acta Crystallogr., Sect. B* **1980**, *36*, 2378–2385; S. Brückner, *Chim. Ind.* **1988**, *70*, 48–53; S. V. Meille, S. Brückner, J. B. Lando, *Polymer* **1989**, *30*, 786–792.
[24] H. M. Rietveld, *J. Appl. Crystallogr.* **1969**, *2*, 65–67.
[25] M. I. Kay, R. A. Young, A. S. Posner, *Nature* **1964**, *204*, 1050–1052.
[26] G. Caglioti, A. Paoletti, F. P. Ricci, *Nucl. Instrum.* **1958**, *3*, 223–228.

Received: May 8, 2006
Published Online: October 5, 2006

